

A FINITE DIFFERENCE SOLUTION OF THE REGULARIZED LONG-WAVE EQUATION

S. KUTLUAY AND A. ESEN

Received 26 July 2005; Accepted 24 January 2006

A linearized implicit finite difference method to obtain numerical solution of the one-dimensional regularized long-wave (RLW) equation is presented. The performance and the accuracy of the method are illustrated by solving three test examples of the problem: a single solitary wave, two positive solitary waves interaction, and an undular bore. The obtained results are presented and compared with earlier work.

Copyright © 2006 S. Kutluay and A. Esen. This is an open access article distributed under the Creative Commons Attribution License, which permits unrestricted use, distribution, and reproduction in any medium, provided the original work is properly cited.

1. Introduction

In this study, we will consider the one-dimensional RLW equation

$$\frac{\partial U}{\partial t} + \frac{\partial U}{\partial x} + \varepsilon U \frac{\partial U}{\partial x} - \mu \frac{\partial}{\partial t} \left(\frac{\partial^2 U}{\partial x^2} \right) = 0, \quad (1.1)$$

with the physical boundary conditions $U \rightarrow 0$ as $x \rightarrow \pm\infty$, where t is time, x is the space coordinate, $U(x, t)$ is the wave amplitude, and ε and μ are positive parameters. The RLW equation (1.1) was first introduced by Peregrine [1] to describe the development of an undular bore. This equation is one of the most important nonlinear wave equations which can be used to model a large number of problems arising in various areas of applied sciences [2, 3]. The RLW equation has been solved analytically for a restricted set of boundary and initial conditions. Therefore, the numerical solution of the RLW equation has been the subject of many papers. Various numerical techniques particularly including finite difference [4–8], finite element [9–19], and spectral [20–23] methods have been used for the solution of the RLW equation.

In this paper, we have used a linearized implicit finite difference method to investigate the motion of a single solitary wave, development of two positive solitary waves interaction, and an undular bore for the RLW equation (1.1).

2 Regularized long-wave equation

2. Method of solution

For the numerical treatment, the spatial variable x of the problem is restricted over an interval $a \leq x \leq b$. In this study, we consider the RLW equation (1.1) with the homogeneous boundary conditions

$$U(a, t) = 0, \quad t > 0, \quad U(b, t) = 0, \quad t > 0, \quad (2.1)$$

and the initial condition

$$U(x, 0) = f(x), \quad a \leq x \leq b, \quad (2.2)$$

where $f(x)$ is a prescribed function.

The solution domain $a \leq x \leq b, t > 0$ is divided into subintervals Δx in the direction of the spatial variable x and Δt in the direction of time t such that $x_i = i\Delta x, i = 0(1)N$ ($N\Delta x = b - a$); $t_j = j\Delta t, j = 0(1)J$, and the numerical solution of U at the grid point $(i\Delta x, j\Delta t)$ is denoted by $U_{i,j}$.

In the finite difference method, the dependent variable and its derivatives are approximated by the finite difference approximation. This approximation will lead to either a single explicit equation or a system of difference equations. Applying the classical implicit finite difference method to nonlinear problems normally gives nonlinear system of equations which cannot be solved directly.

Equation (1.1) can be written as

$$\frac{\partial U}{\partial t} + \frac{\partial U}{\partial x} + \frac{\varepsilon}{2} \frac{\partial U^2}{\partial x} - \mu \frac{\partial}{\partial t} \left(\frac{\partial^2 U}{\partial x^2} \right) = 0. \quad (2.3)$$

Using the forward difference approximation for $\partial U/\partial t$, the Crank-Nicolson difference approximation for $\partial U/\partial x$ and $\partial U^2/\partial x$, and the central difference approximation for $\partial^2 U/\partial x^2$ at the point $(i, j + 1)$,

$$\begin{aligned} \frac{\partial U}{\partial t} &\cong \frac{U_{i,j+1} - U_{i,j}}{\Delta t}, \\ \frac{\partial U}{\partial x} &\cong \frac{1}{2} \left\{ \frac{1}{2\Delta x} (U_{i+1,j+1} - U_{i-1,j+1}) + \frac{1}{2\Delta x} (U_{i+1,j} - U_{i-1,j}) \right\}, \\ \frac{\partial U^2}{\partial x} &\cong \frac{1}{2} \left\{ \frac{1}{2\Delta x} (U_{i+1,j+1}^2 - U_{i-1,j+1}^2) + \frac{1}{2\Delta x} (U_{i+1,j}^2 - U_{i-1,j}^2) \right\}, \\ \frac{\partial^2 U}{\partial x^2} &\cong \frac{1}{(\Delta x)^2} (U_{i+1,j} - 2U_{i,j} + U_{i-1,j}), \end{aligned} \quad (2.4)$$

respectively, (2.3) yields the system of algebraic equations

$$\begin{aligned} &\frac{U_{i,j+1} - U_{i,j}}{\Delta t} + \frac{1}{4\Delta x} (U_{i+1,j+1} - U_{i-1,j+1} + U_{i+1,j} - U_{i-1,j}) \\ &+ \frac{\varepsilon}{8\Delta x} (U_{i+1,j+1}^2 - U_{i-1,j+1}^2 + U_{i+1,j}^2 - U_{i-1,j}^2) \\ &- \frac{\mu}{\Delta t (\Delta x)^2} (U_{i+1,j+1} - 2U_{i,j+1} + U_{i-1,j+1} - U_{i+1,j} + 2U_{i,j} - U_{i-1,j}) = 0 \end{aligned} \quad (2.5)$$

for $i = 1(1)N - 1$ and $j = 0(1)J$ with a truncation error of $O(\Delta t) + O(\Delta x)^2$. The scheme is a nonlinear system of equations in $U_{i,j+1}$ and it needs to use an iteration technique to evaluate the solution.

Using the central difference operator δ defined by $\delta_x U_{i,j} = U_{i+1,j} - U_{i-1,j}$, (2.5) can be written as

$$\begin{aligned} & \frac{U_{i,j+1} - U_{i,j}}{\Delta t} + \frac{1}{4\Delta x} (U_{i+1,j+1} - U_{i-1,j+1} + U_{i+1,j} - U_{i-1,j}) \\ & + \frac{\varepsilon}{8\Delta x} \{ \delta_x (U_{i,j+1}^2) + \delta_x (U_{i,j}^2) \} \\ & - \frac{\mu}{\Delta t (\Delta x)^2} (U_{i+1,j+1} - 2U_{i,j+1} + U_{i-1,j+1} - U_{i+1,j} + 2U_{i,j} - U_{i-1,j}) = 0. \end{aligned} \quad (2.6)$$

By Taylor expansion of $U_{i,j+1}^2$ about the point (i, j) we obtain

$$U_{i,j+1}^2 = U_{i,j}^2 + \Delta t \frac{\partial U_{i,j}^2}{\partial t} + \dots = U_{i,j}^2 + \Delta t \frac{\partial U_{i,j}^2}{\partial U_{i,j}} \frac{\partial U_{i,j}}{\partial t} + \dots \quad (2.7)$$

Hence in terms of order Δt , $U_{i,j+1}^2 \cong U_{i,j}^2 + 2U_{i,j}(U_{i,j+1} - U_{i,j})$, and taking

$$W_i = U_{i,j+1} - U_{i,j}, \quad (2.8)$$

(2.6), with some manipulations, leads to

$$\begin{aligned} & \left(\frac{\varepsilon}{4\Delta x} U_{i-1,j} + \frac{\mu}{\Delta t (\Delta x)^2} + \frac{1}{4\Delta x} \right) W_{i-1} - \left(\frac{1}{\Delta t} + \frac{2\mu}{\Delta t (\Delta x)^2} \right) W_i \\ & + \left(\frac{\mu}{\Delta t (\Delta x)^2} - \frac{1}{4\Delta x} U_{i+1,j} - \frac{1}{4\Delta x} \right) W_{i+1} \\ & = \frac{1}{2\Delta x} (U_{i+1,j} - U_{i-1,j}) + \frac{\varepsilon}{4\Delta x} (U_{i+1,j}^2 - U_{i-1,j}^2), \end{aligned} \quad (2.9)$$

($i = 1(1)N - 1$) a system of linear equations for W_i . This approximation is second order in both space and time as regards truncation error. Obviously, the solution at the $(j + 1)$ th time level is obtained from (2.8) as $U_{i,j+1} = U_{i,j} + W_i$. Since the stability parameter $\Delta t/(\Delta x)^2$ depends not only on the form of the finite difference scheme (2.9) but also generally upon the solution $U(x, t)$ being obtained, the complications and difficulties may arise in the analysis of stability. In order to show how good the numerical solutions are in comparison with the exact ones, we will use the L_2 and L_∞ error norms defined by

$$\begin{aligned} L_2 &= \|U^{\text{exact}} - U^{\text{num}}\|_2 = \left[\Delta x \sum_{i=1}^N |U_i^{\text{exact}} - U_i^{\text{num}}|^2 \right]^{1/2}, \\ L_\infty &= \|U^{\text{exact}} - U^{\text{num}}\|_\infty = \max_i |U_i^{\text{exact}} - U_i^{\text{num}}|. \end{aligned} \quad (2.10)$$

3. Numerical examples and results

All computations were executed on a Pentium 4 PC in the Fortran code using double precision arithmetic. The RLW equation (1.1) satisfies only three conservation laws given as

$$\begin{aligned}
 I_1 &= \int_{-\infty}^{+\infty} U dx \simeq \Delta x \sum_{i=1}^N U_{i,j}, \\
 I_2 &= \int_{-\infty}^{+\infty} [U^2 + \mu(U_x)^2] dx \simeq \Delta x \sum_{i=1}^N [(U_{i,j})^2 + \mu((U_x)_{i,j})^2], \\
 I_3 &= \int_{-\infty}^{+\infty} [U^3 + 3U^2] dx \simeq \Delta x \sum_{i=1}^N [(U_{i,j})^3 + 3(U_{i,j})^2]
 \end{aligned} \tag{3.1}$$

which respectively correspond to mass, momentum, and energy [24]. In the simulations the invariants I_1 , I_2 , and I_3 are monitored to check the conservation of the numerical scheme. For the computation of U_x in (3.1), we used a central finite difference approximation.

To implement the performance of the method, three test problems will be considered: the motion of a single solitary wave, the interaction of two positive solitary waves, and the undular bore.

3.1. The motion of a single solitary wave. We first consider (1.1) with the boundary conditions $U \rightarrow 0$ as $x \rightarrow \pm\infty$ and the initial condition

$$U(x, 0) = 3c \operatorname{sech}^2(k(x - x_0)). \tag{3.2}$$

The exact solution of this problem is

$$U(x, t) = 3c \operatorname{sech}^2(k(x - vt - x_0)). \tag{3.3}$$

This solution corresponds to the motion of a single solitary wave with amplitude $3c$ and width k , initially centered at x_0 , where $v = 1 + \varepsilon c$ is the wave velocity and $k = (1/2)(\varepsilon c/\mu v)^{1/2}$. This solution will also be used over an interval $a \leq x \leq b$. For this problem the theoretical values of the invariants are [14]

$$I_1 = \frac{6c}{k}, \quad I_2 = \frac{12c^2}{k} + \frac{48kc^2\mu}{5}, \quad I_3 = \frac{36c^2}{k} + \frac{144c^3}{5k} \tag{3.4}$$

which are recorded throughout the simulations. For the purpose of comparing with the earlier work, all computations are done for the parameters $\varepsilon = 1$, $\mu = 1$, and $x_0 = 0$.

Table 3.1 displays a comparison of the values of the invariants and error norms obtained by the present method with those obtained using the cubic finite difference method developed by Jain et al. [6] and implemented by Gardner et al. [10] for $c = 0.1$. As it is seen from the table, the numerical values of invariants obtained from (3.1) are in very good agreement with their analytical values obtained from (3.4). The quantities in the invariants remain almost constant during the computer run. For the proposed finite difference

Table 3.1. Invariants and error norms for the single soliton with $c = 0.1$, $\Delta x = 0.1$, $\Delta t = 0.1$, and over the region $-40 \leq x \leq 60$.

| t | I_1 | I_2 | I_3 | $L_2 \times 10^3$ | $L_\infty \times 10^3$ |
|--|---------|----------|---------|-------------------|------------------------|
| Present method | | | | | |
| 0 | 3.97992 | 0.810459 | 2.57901 | 0.00 | 0.00 |
| 4 | 3.97995 | 0.810459 | 2.57901 | 0.12 | 0.05 |
| 8 | 3.97997 | 0.810459 | 2.57901 | 0.23 | 0.09 |
| 12 | 3.97999 | 0.810459 | 2.57901 | 0.34 | 0.14 |
| 16 | 3.97999 | 0.810459 | 2.57901 | 0.45 | 0.18 |
| 20 | 3.97997 | 0.810459 | 2.57901 | 0.55 | 0.21 |
| Finite difference cubic method [6, 10] | | | | | |
| 0 | 3.97992 | 0.810459 | 2.57901 | 0.00 | 0.00 |
| 4 | 4.42017 | 0.899873 | 2.86339 | 39.82 | 13.74 |
| 8 | 4.41822 | 0.899236 | 2.86106 | 79.46 | 27.66 |
| 12 | 4.41623 | 0.898601 | 2.85863 | 118.8 | 41.35 |
| 16 | 4.41423 | 0.897967 | 2.85613 | 157.7 | 54.60 |
| 20 | 4.41219 | 0.897342 | 2.85361 | 196.1 | 67.35 |

method at times $t = 0$ and $t = 20$, change in I_1 is 0.5×10^{-4} , and I_2 and I_3 are exact up to the last recorded digit, whereas for the cubic finite difference method, they are 0.43227, 0.086883, and 0.2746, respectively. The error norms at each time obtained by the present method are smaller than those given in [6, 10]. For the present method at $t = 20$, the error norms are $L_2 = 0.55 \times 10^{-3}$ and $L_\infty = 0.21 \times 10^{-3}$, whereas they are $L_2 = 196.1 \times 10^{-3}$ and $L_\infty = 67.35 \times 10^{-3}$ for the cubic finite difference method. In Table 3.2 the time evolution of the invariants I_1 , I_2 , and I_3 , and of the error norms L_2 and L_∞ for $c = 0.03$, is compared with the cubic finite difference method [6, 10]. Again the present method produces good results.

The rates of convergence for the proposed numerical method in space sizes Δx_m and time steps Δt_m can be calculated by

$$\text{Order} = \frac{\log_{10} (|U^{\text{exact}} - U_{\Delta x_m}^{\text{num}}| / |U^{\text{exact}} - U_{\Delta x_{m+1}}^{\text{num}}|)}{\log_{10} (\Delta x_m / \Delta x_{m+1})}, \quad (3.5)$$

$$\text{Order} = \frac{\log_{10} (|U^{\text{exact}} - U_{\Delta t_m}^{\text{num}}| / |U^{\text{exact}} - U_{\Delta t_{m+1}}^{\text{num}}|)}{\log_{10} (\Delta t_m / \Delta t_{m+1})},$$

respectively [18].

The convergence rates computed by the present method for values of space size Δx_m and a fixed value of the time step Δt are recorded in Table 3.3. It is clearly seen that the scheme provides remarkable reductions in convergence rates for the smaller space sizes.

6 Regularized long-wave equation

Table 3.2. Invariants and error norms for the single soliton with $c = 0.03$, $\Delta x = 0.1$, $\Delta t = 0.1$, and over the region $-40 \leq x \leq 60$.

| t | I_1 | I_2 | I_3 | $L_2 \times 10^3$ | $L_\infty \times 10^3$ |
|--|-------|-----------|-----------|-------------------|------------------------|
| Present method | | | | | |
| 0 | 2.107 | 0.127 301 | 0.388 804 | 0.000 | 0.000 |
| 4 | 2.108 | 0.127 302 | 0.388 806 | 0.150 | 0.123 |
| 8 | 2.109 | 0.127 302 | 0.388 807 | 0.321 | 0.166 |
| 12 | 2.110 | 0.127 302 | 0.388 807 | 0.467 | 0.179 |
| 16 | 2.110 | 0.127 302 | 0.388 808 | 0.567 | 0.185 |
| 20 | 2.109 | 0.127 302 | 0.388 807 | 0.638 | 0.233 |
| Finite difference cubic method [6, 10] | | | | | |
| 0 | 2.107 | 0.127 301 | 0.388 804 | 0.000 | 0.000 |
| 4 | 2.340 | 0.141 322 | 0.431 621 | 2.928 | 0.786 |
| 8 | 2.339 | 0.141 195 | 0.431 231 | 5.816 | 1.582 |
| 12 | 2.337 | 0.141 067 | 0.430 834 | 8.698 | 2.384 |
| 16 | 2.336 | 0.140 940 | 0.430 440 | 11.58 | 3.190 |
| 20 | 2.333 | 0.140 815 | 0.430 052 | 14.45 | 3.996 |

Table 3.3. The order of convergence at $t = 20$, $\Delta t = 0.1$, $c = 0.1$ ($-40 \leq x \leq 60$), and $c = 0.03$ ($-80 \leq x \leq 120$).

| c | Δx_j | $L_2 \times 10^3$ | Order | $L_\infty \times 10^3$ | Order |
|------|--------------|-------------------|-----------|------------------------|-----------|
| 0.1 | 1 | 33.666 68 | — | 12.748 33 | — |
| | 0.5 | 8.767 886 | 1.941 021 | 3.381 133 | 1.914 730 |
| | 0.25 | 2.358 203 | 1.894 541 | 0.910 513 | 1.892 755 |
| | 0.125 | 0.744 691 | 1.662 974 | 0.286 720 | 1.667 037 |
| | 0.025 | 0.229 367 | 0.731 713 | 0.086 429 | 0.745 094 |
| | 0.0125 | 0.213 601 | 0.102 739 | 0.080 163 | 0.108 579 |
| 0.03 | 1 | 2.620 662 | — | 0.794 513 | — |
| | 0.5 | 0.667 923 | 1.972 178 | 0.202 298 | 1.973 589 |
| | 0.25 | 0.177 379 | 1.912 847 | 0.053 656 | 1.914 671 |
| | 0.125 | 0.054 606 | 1.699 704 | 0.016 471 | 1.703 811 |
| | 0.025 | 0.015 359 | 0.788 127 | 0.004 569 | 0.796 742 |
| | 0.0125 | 0.014 146 | 0.118 690 | 0.004 198 | 0.122 176 |

Table 3.4 displays the computed convergence rates for various values of time step Δt_j and a fixed value of the space size Δx . Again a noticeable decrease in convergence rates is observed when the time step decreases.

Table 3.4. The order of convergence at $t = 20$, $\Delta x = 0.1$, $c = 0.1$ ($-40 \leq x \leq 60$), and $c = 0.03$ ($-80 \leq x \leq 120$).

| c | Δt_j | $L_2 \times 10^3$ | Order | $L_\infty \times 10^3$ | Order |
|------|--------------|-------------------|-----------|------------------------|-----------|
| 0.1 | 1 | 20.292 460 | — | 7.618 319 | — |
| | 0.5 | 5.461 549 | 1.893 562 | 2.062 621 | 1.884 994 |
| | 0.25 | 1.631 432 | 1.743 171 | 6.197 000 | 1.734 837 |
| | 0.125 | 0.666 724 | 1.290 977 | 0.255 439 | 1.278 591 |
| | 0.025 | 0.358 400 | 0.385 679 | 0.138 568 | 0.380 022 |
| | 0.0125 | 0.348 799 | 0.039 175 | 0.134 914 | 0.038 554 |
| 0.03 | 1 | 1.380 075 | — | 0.411 315 | — |
| | 0.5 | 0.367 151 | 1.910 301 | 0.109 469 | 1.909 721 |
| | 0.25 | 0.111 587 | 1.718 205 | 0.033 363 | 1.714 201 |
| | 0.125 | 0.047 558 | 1.230 409 | 0.014 296 | 1.222 637 |
| | 0.025 | 0.027 068 | 0.350 183 | 0.008 194 | 0.345 821 |
| | 0.0125 | 0.026 428 | 0.034 521 | 0.008 003 | 0.034 027 |

The profiles of the solitary waves at times $t = 0$ and $t = 20$ and the error distributions of the analytical and numerical solutions at $t = 20$ for $c = 0.1$ with the range $-40 \leq x \leq 60$ and for $c = 0.03$ with the range $-80 \leq x \leq 120$, $\Delta x = 0.125$ and $\Delta t = 0.1$ are shown in Figure 3.1. For $c = 0.1$, the amplitude is 0.3 at time $t = 0$ while it is 0.299919 at time $t = 20$ (Figure 3.1(a)) and so the relative change in the amplitude is about 0.027%. It is seen that the maximum error is about between -4×10^{-3} and 4×10^{-3} (Figure 3.1(b)). For $c = 0.03$, the amplitude is 0.09 at time $t = 0$ while it is 0.089997 at time $t = 20$ (Figure 3.1(c)) and so the relative change in the amplitude is about 0.0033%. It is observed that the maximum error is about between -6×10^{-4} and 6×10^{-4} (Figure 3.1(d)).

3.2. The interaction of two positive solitary waves. We secondly consider (1.1) with the boundary conditions $U \rightarrow 0$ as $x \rightarrow \pm\infty$ and the initial condition [17]

$$U(x, 0) = \sum_{j=1}^2 3A_j \operatorname{sech}^2(k_j(x - x_j)), \quad (3.6)$$

where $A_j = 4k_j^2/(1 - 4k_j^2)$ ($j = 1, 2$).

For the simulation, all computations are done for the parameters $k_1 = 0.4$, $x_1 = 15$, $k_2 = 0.3$, $x_2 = 35$, $\varepsilon = 1$, $\mu = 1$, $\Delta x = 0.3$, and $\Delta t = 0.1$ over the region $0 \leq x \leq 120$. The experiment was run from $t = 0$ to $t = 25$ to allow the interaction to take place. Figure 3.2 shows the interaction of two positive solitary waves. As it is seen from the figure, at $t = 0$ a solitary wave with larger amplitude is on the left of the other solitary wave with smaller amplitude. The larger wave catches up with the smaller one as the time increases. At $t = 0$,

8 Regularized long-wave equation

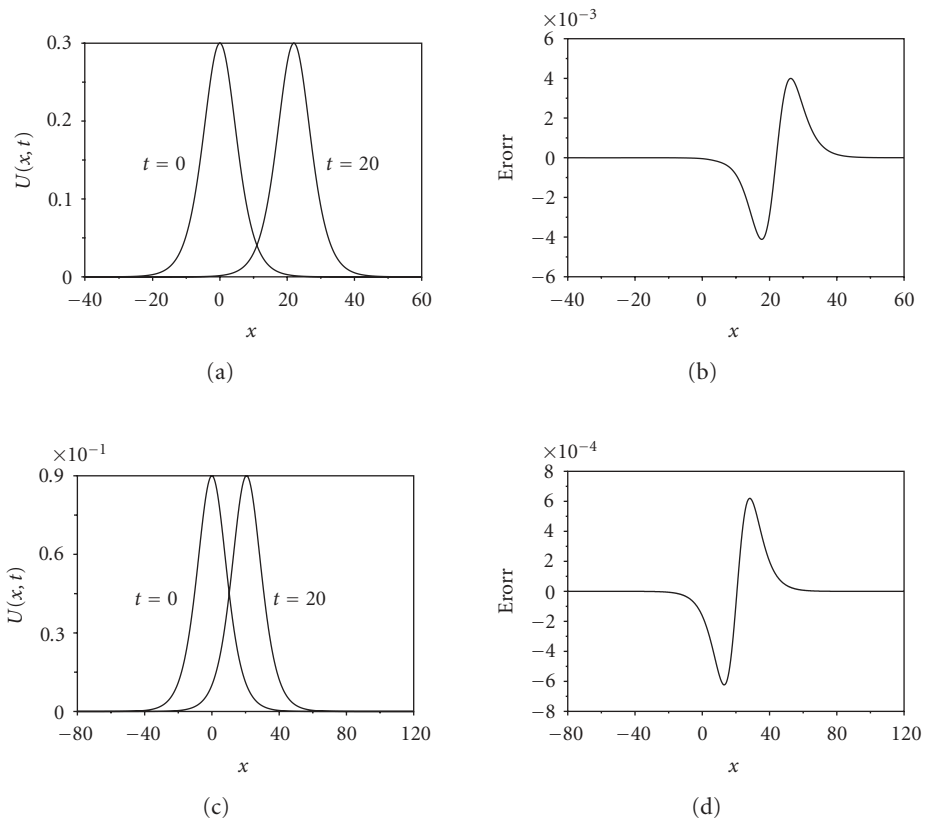


Figure 3.1. Solitary wave profiles at $t = 0, 20$ and error (error = exact-numerical) distributions at $t = 20$.

the amplitude of the larger solitary wave is 5.33338 while the amplitude of the smaller one is 1.68598, whereas at $t = 25$, the amplitude of the larger solitary wave is 5.30235 at the point $x = 86.7$ while the amplitude of the smaller one is 1.67157 at the point $x = 69.9$. An oscillation of small amplitude trailing behind the solitary waves was observed. In order to see this oscillation occurring behind the waves in Figure 3.2 at time $t = 25$, the scale of the figure is magnified as in Figure 3.3. It is clearly seen that an oscillation of amplitude $\sim 2.2 \times 10^{-2}$ is trailing behind the solitary waves.

Table 3.5 displays a comparison of the values of the invariants obtained by the present method with those obtained in [17]. It is observed that the obtained values of the invariants remain almost constant during the computer run. At times $t = 0$ and $t = 25$, the relative changes in the invariants I_1 , I_2 , and I_3 for the present method are respectively $2.558 \times 10^{-3}\%$, $6.647 \times 10^{-3}\%$, and $9.797 \times 10^{-3}\%$ whereas they are 0.352%, 0.570%, and 2.237% for the cubic B-spline collocation finite element method given in [17]. It is clearly seen that each of the conserved quantities obtained by the present method is very well preserved.

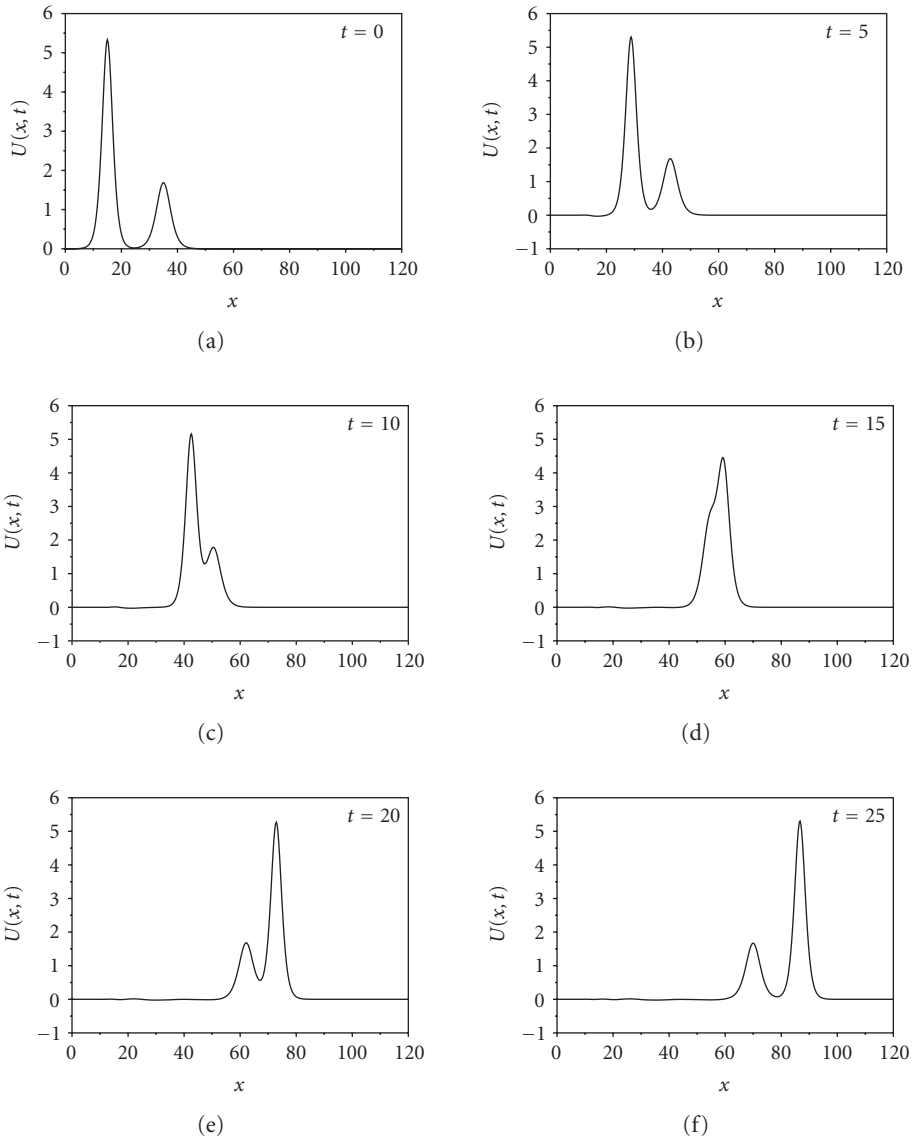


Figure 3.2. The interaction of two positive solitary waves at different times.

3.3. The undular bore. As our last test problem, we consider (1.1) with the physical boundary conditions $U \rightarrow 0$ as $x \rightarrow \infty$ and $U \rightarrow U_0$ as $x \rightarrow -\infty$, and the initial condition

$$U(x,0) = \frac{U_0}{2} \left[1 - \tanh\left(\frac{x-x_0}{d}\right) \right], \quad (3.7)$$

10 Regularized long-wave equation

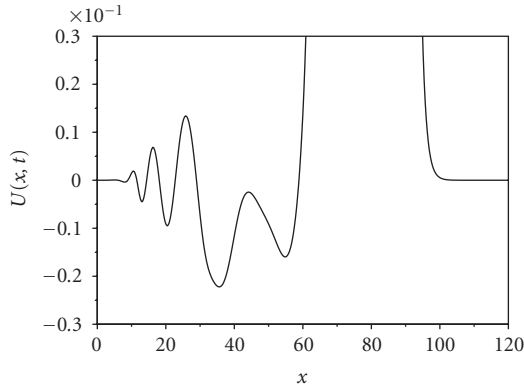


Figure 3.3. The interaction of two solitary waves at $t = 25$ in Figure 3.2 (magnified).

where $U(x, 0)$, denotes the elevation of the water surface above the equilibrium level at time $t = 0$, U_0 represents the magnitude of the change in water level which is centered on $x = x_0$, and d measures the steepness of the change. Under the above physical boundary conditions, the invariants I_1, I_2, I_3 are not constant but increase linearly throughout the simulation at the following rates [14]:

$$\begin{aligned}
 M_1 &= \frac{d}{dt} I_1 = \frac{d}{dt} \int_{-\infty}^{+\infty} U \, dx = U_0 + \frac{1}{2} U_0^2, \\
 M_2 &= \frac{d}{dt} I_2 = \frac{d}{dt} \int_{-\infty}^{+\infty} \{U^2 + \mu(U_x)^2\} \, dx = U_0^2 + \frac{2}{3} U_0^3, \\
 M_3 &= \frac{d}{dt} I_3 = \frac{d}{dt} \int_{-\infty}^{+\infty} (U^3 + 3U^2) \, dx = 3U_0^2 + 3U_0^3 + \frac{3}{4} U_0^4,
 \end{aligned} \tag{3.8}$$

respectively.

For the simulation, all computations are done for the parameters $\varepsilon = 1.5$, $\mu = 1/6$, $U_0 = 0.1$, $x_0 = 0$, $\Delta x = 0.24$, $\Delta t = 0.1$, and $d = 2, 5$ in the region $-36 \leq x \leq 300$. The simulation is run until time $t = 250$, and the values of the quantities I_1, I_2, I_3 with the position and amplitude of the leading undulation for the steep slope $d = 2$ and the gentle slope $d = 5$ are recorded in Table 3.6. The numerical values of variations in quantities I_1, I_2, I_3 are obtained as $M_1 = 0.107500$, $M_2 = 0.010992$, $M_3 = 0.034096$ for $d = 2$ and $M_1 = 0.107500$, $M_2 = 0.010992$, $M_3 = 0.034101$ for $d = 5$ which are in good agreement with the theoretical values $M_1 = 0.105000$, $M_2 = 0.010667$, $M_3 = 0.033075$ obtained from (3.8). The values of I_1, I_2 , and I_3 increase linearly according to the values of M_1, M_2 , and M_3 , respectively. The amplitudes of the leading undulation for $d = 5$ and $d = 2$ are 0.17710 and 0.18158, respectively.

Table 3.5. Invariants for the interaction of two positive solitary waves.

| t | I_1 | I_2 | I_3 | I_1 [17] | I_2 [17] | I_3 [17] |
|-----|-----------|------------|------------|------------|------------|------------|
| 0 | 37.916 48 | 120.351 50 | 744.081 40 | 37.916 52 | 120.522 80 | 744.081 50 |
| 2 | 37.916 82 | 120.357 10 | 744.038 70 | 37.915 96 | 119.178 30 | 725.545 80 |
| 4 | 37.916 97 | 120.358 40 | 744.011 00 | 37.911 70 | 121.160 20 | 736.944 30 |
| 5 | 37.917 04 | 120.358 60 | 743.998 50 | — | — | — |
| 6 | 37.917 09 | 120.358 30 | 743.979 60 | 37.896 62 | 118.126 60 | 714.058 40 |
| 8 | 37.917 19 | 120.357 00 | 743.867 90 | 37.859 75 | 119.731 70 | 728.517 30 |
| 10 | 37.917 27 | 120.363 80 | 743.420 20 | 37.792 21 | 119.734 30 | 726.687 90 |
| 12 | 37.917 33 | 120.391 50 | 742.338 70 | 37.696 67 | 119.633 40 | 725.723 60 |
| 14 | 37.917 36 | 120.415 60 | 741.578 10 | 37.595 53 | 119.235 90 | 724.700 20 |
| 15 | 37.917 38 | 120.406 00 | 741.891 50 | — | — | — |
| 16 | 37.917 40 | 120.388 60 | 742.488 90 | 37.529 16 | 119.418 50 | 725.839 90 |
| 18 | 37.917 41 | 120.365 30 | 743.475 20 | 37.540 27 | 119.827 60 | 727.088 60 |
| 20 | 37.917 44 | 120.359 90 | 743.863 80 | 37.647 30 | 119.804 10 | 727.194 80 |
| 22 | 37.917 45 | 120.359 40 | 743.975 00 | 37.822 37 | 119.798 20 | 727.254 20 |
| 24 | 37.917 46 | 120.359 50 | 744.003 70 | 37.993 13 | 119.892 30 | 727.492 10 |
| 25 | 37.917 45 | 120.359 50 | 744.008 50 | 38.050 10 | 119.835 50 | 727.439 20 |

Table 3.6. Invariants, position, and amplitude of the leading undulation for $d = 2, 5$.

| d | t | I_1 | I_2 | I_3 | x | Amplitude |
|-----|-----|-----------|----------|----------|------------|-----------|
| 2 | 0 | 3.588 00 | 0.350 81 | 1.080 78 | — | — |
| | 50 | 8.963 00 | 0.899 05 | 2.785 84 | 48.960 00 | 0.139 40 |
| | 100 | 14.337 99 | 1.449 01 | 4.490 69 | 102.480 00 | 0.158 31 |
| | 150 | 19.713 01 | 1.998 96 | 6.195 43 | 156.720 00 | 0.170 13 |
| | 200 | 25.087 99 | 2.548 92 | 7.900 13 | 211.200 00 | 0.177 13 |
| | 250 | 30.462 99 | 3.098 87 | 9.604 82 | 265.680 00 | 0.181 58 |
| 5 | 0 | 3.588 00 | 0.335 65 | 1.033 53 | — | — |
| | 50 | 8.963 00 | 0.883 91 | 2.739 02 | 48.240 00 | 0.110 67 |
| | 100 | 14.338 01 | 1.433 89 | 4.444 24 | 102.240 00 | 0.136 83 |
| | 150 | 19.713 00 | 1.983 85 | 6.149 18 | 156.240 00 | 0.157 14 |
| | 200 | 25.088 02 | 2.533 81 | 7.853 95 | 210.480 00 | 0.169 90 |
| | 250 | 30.463 05 | 3.083 76 | 9.558 68 | 264.960 00 | 0.177 10 |

12 Regularized long-wave equation

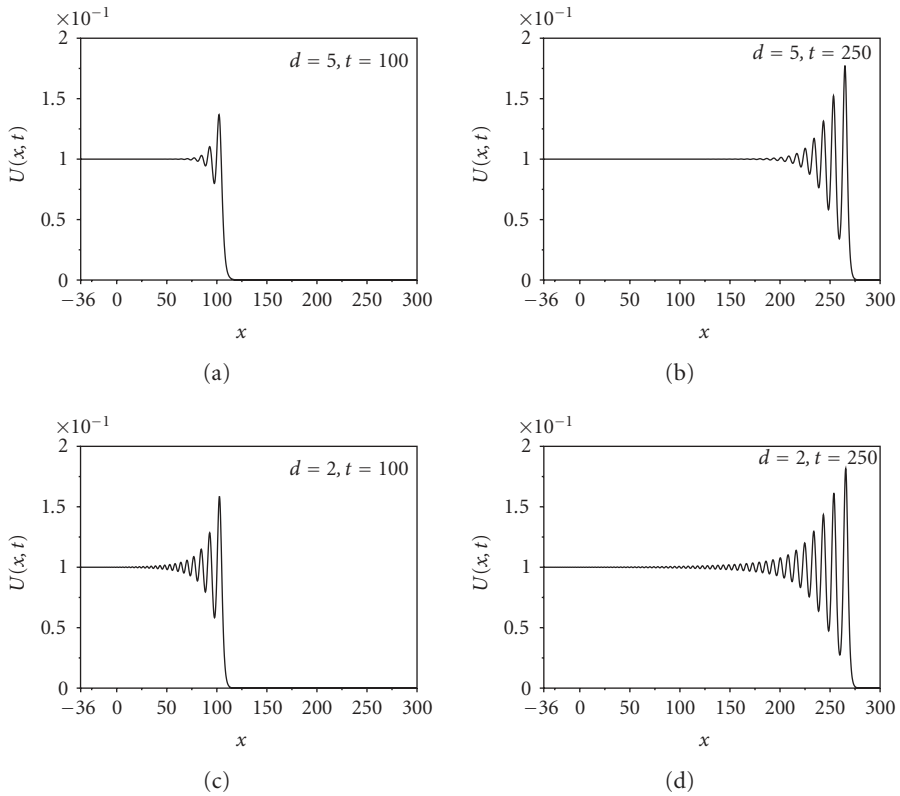


Figure 3.4. Undulation profiles for the gentle slope $d = 5$ and steep slope $d = 2$ at $t = 100$ and $t = 250$.

Figure 3.4 illustrates the undular bore profiles at $t = 100$ and $t = 250$ for the gentle slope $d = 5$ and the steep slope $d = 2$. As it can be seen that from the figure, the number of undulations formed increases with the decrease of d from $d = 5$ to $d = 2$. The number of undulations also increases with the increase of t , as expected.

4. Conclusion

A linearized implicit finite difference method was presented to obtain numerical solutions of the RLW equation. The efficiency of the method was tested on three numerical experiments of wave propagation: the motion of a single solitary wave, the development of two positive solitary waves interaction, and an undular bore, and its accuracy was examined by the error norms L_2 and L_∞ . The obtained results show that the error norms are reasonably small and the conservation properties are all very good. The results also suggest that the present method whose application is easier than many other numerical techniques such as finite element and spectral methods can be applied to a large number of physically important nonlinear wave problems with success.

References

- [1] D. H. Peregrine, *Calculations of the development of an undular bore*, Journal of Fluid Mechanics **25** (1966), 321–330.
- [2] T. B. Benjamin, J. L. Bona, and J. J. Mahony, *Model equations for long waves in nonlinear dispersive systems*, Philosophical Transactions of the Royal Society of London. Series A **272** (1972), no. 1220, 47–78.
- [3] J. L. Bona and P. J. Bryant, *A mathematical model for long waves generated by wavemakers in non-linear dispersive systems*, Proceedings of the Cambridge Philosophical Society **73** (1973), 391–405.
- [4] P. C. Jain and L. Iskandar, *Numerical solutions of the regularized long-wave equation*, Computer Methods in Applied Mechanics and Engineering **20** (1979), no. 2, 195–201.
- [5] J. C. Eilbeck and G. R. McGuire, *Numerical study of the regularized long-wave equation. II. Interaction of solitary waves*, Journal of Computational Physics **23** (1977), no. 1, 63–73.
- [6] P. C. Jain, R. Shankar, and T. V. Singh, *Numerical solution of regularized long-wave equation*, Communications in Numerical Methods in Engineering **9** (1993), no. 7, 579–586.
- [7] D. Bhardwaj and R. Shankar, *A computational method for regularized long wave equation*, Computers & Mathematics with Applications **40** (2000), no. 12, 1397–1404.
- [8] Q. S. Chang, G. B. Wang, and B. L. Guo, *Conservative scheme for a model of nonlinear dispersive waves and its solitary waves induced by boundary motion*, Journal of Computational Physics **93** (1991), no. 2, 360–375.
- [9] L. R. T. Gardner and G. A. Gardner, *Solitary waves of the regularised long-wave equation*, Journal of Computational Physics **91** (1990), no. 2, 441–459.
- [10] L. R. T. Gardner, G. A. Gardner, and I. Dag, *A B-spline finite element method for the regularized long wave equation*, Communications in Numerical Methods in Engineering **11** (1995), no. 1, 59–68.
- [11] I. Dag, *Least-squares quadratic B-spline finite element method for the regularised long wave equation*, Computer Methods in Applied Mechanics and Engineering **182** (2000), no. 1-2, 205–215.
- [12] I. Dag and M. N. Özer, *Approximation of RLW equation by least square cubic B-spline finite element method*, Applied Mathematical Modelling **25** (2001), no. 3, 221–231.
- [13] A. Dogan, *Numerical solution of RLW equation using linear finite elements within Galerkin's method*, Applied Mathematical Modelling **26** (2002), no. 7, 771–783.
- [14] S. I. Zaki, *Solitary waves of the splitted RLW equation*, Computer Physics Communications **138** (2001), no. 1, 80–91.
- [15] I. Dag, B. Saka, and D. Irk, *Application of cubic B-splines for numerical solution of the RLW equation*, Applied Mathematics and Computation **159** (2004), no. 2, 373–389.
- [16] A. A. Soliman and K. R. Raslan, *Collocation method using quadratic B-spline for the RLW equation*, International Journal of Computer Mathematics **78** (2001), no. 3, 399–412.
- [17] K. R. Raslan, *A computational method for the regularized long wave (RLW) equation*, Applied Mathematics and Computation **167** (2005), no. 2, 1101–1118.
- [18] I. Dag, B. Saka, and D. Irk, *Galerkin method for the numerical solution of the RLW equation using quintic B-splines*, Journal of Computational and Applied Mathematics **190** (2006), no. 1-2, 532–547.
- [19] B. Y. Guo and W. M. Cao, *The Fourier pseudospectral method with a restrain operator for the RLW equation*, Journal of Computational Physics **74** (1988), no. 1, 110–126.
- [20] B. Y. Guo and V. S. Manoranjan, *Spectral method for solving the RLW equation*, Journal of Computational Mathematics **3** (1985), no. 3, 228–237.
- [21] D. M. Sloan, *Fourier pseudospectral solution of the regularised long wave equation*, Journal of Computational and Applied Mathematics **36** (1991), no. 2, 159–179.

14 Regularized long-wave equation

- [22] K. Djidjeli, W. G. Price, E. H. Twizell, and Q. Cao, *A linearized implicit pseudo-spectral method for some model equations: the regularized long wave equations*, Communications in Numerical Methods in Engineering **19** (2003), no. 11, 847–863.
- [23] P. M. Prenter, *Splines and Variational Methods*, Wiley-Interscience, New York, 1975.
- [24] P. J. Olver, *Euler operators and conservation laws of the BBM equation*, Mathematical Proceedings of the Cambridge Philosophical Society **85** (1979), no. 1, 143–160.

S. Kutluay: Department of Mathematics, Faculty of Arts and Science, Inonu University,
44280 Malatya, Turkey
E-mail address: skutluay@inonu.edu.tr

A. Esen: Department of Mathematics, Faculty of Arts and Science, Inonu University,
44280 Malatya, Turkey
E-mail address: aesen@inonu.edu.tr



Hindawi

Submit your manuscripts at
<http://www.hindawi.com>

